Ultrafast hot-electron induced quenching of Tb 4 f magnetic order

Tom Ferté, Nicolas Bergeard, G. Malinowski, R. Abrudan, T. Kachel, K. Holldack, Michel Hehn, Christine Boeglin

Ultrafast hot-electron induced quenching of Tb 4f magnetic order

T. Ferté,[1] N. Bergeard,[1] G. Malinowski,[2] R. Abrudan,[3] T. Kachel,[3] K. Holldack,[3] M. Hehn,[2] and C. Boeglin[1]

[1]*Université de Strasbourg, CNRS, Institut de Physique et Chimie des Matériaux de Strasbourg, UMR 7504, F-67000 Strasbourg, France*

[2]*Institut Jean Lamour, Université Henri Poincaré, Nancy, France*

[3]*Institut für Methoden und Instrumentierung der Forschung mit Synchrotronstrahlung, Helmholtz-Zentrum Berlin für Materialien und Energie GmbH, Albert-Einstein-Strasse 15, 12489 Berlin, Germany*

(Received 7 April 2017; revised manuscript received 1 September 2017; published 23 October 2017)

We have investigated ultrafast quenching of the Tb 4f magnetic order in $Co_{74}Tb_{26}$ alloys, induced by femtosecond hot-electron pulses. The hot-electron pulses were produced in specific nonmagnetic capping layers by infrared femtosecond laser pulses. Our experimental results show that subpicosecond dynamics of Tb 4f magnetic moments can be induced by nonthermal and thermal hot-electron. We further demonstrate that the demagnetization efficiencies of nonthermal and thermal hot-electron are similar. However, the characteristic demagnetization times show values of 0.35 ps for nonthermal hot-electron excitations and 1.2 ps for thermal hot-electron excitations. We explain this temporal elongation by the propagation time of thermal hot-electron through the 15-nm-thick CoTb film.

DOI: 10.1103/PhysRevB.96.144427

I. INTRODUCTION

Determining the ultimate speed for deterministic control of magnetization manipulation is a hot topic in modern magnetism, mainly due to technological application in data manipulation [1]. In this context, the discovery in 1996 [2] of ultrafast magnetization quenching upon femtosecond laser excitation has driven intensive experimental and theoretical works [3]. In the framework of the thermodynamic three-temperature model (3TM), the laser pulse injects its energy in the electronic system that relaxes due to the coupling with the lattice (electron-phonon coupling) and with the spins (electron-spin coupling) [2]. At the subpicosecond time scale, the actual phenomenological model as proposed by Beaurepaire *et al.* addresses neither the conservation of the angular momentum nor the microscopic mechanisms driving the dissipation of the angular momentum [2]. However, both aspects are heavily debated in many experimental and theoretical works. In 2010, Koopmans *et al.* proposed a microscopic 3TM in which spin-flips resulting from the collision between laser-excited electrons with phonons and/or impurities were introduced to account for the angular momentum conservation [4]. Even though this model accurately reproduced some trends of the demagnetization in transition metal [5,6], rare-earth elements [4], and in many magnetic alloys [7–9], doubts have been cast upon the efficiency of spin-flip scattering in ultrafast demagnetization [10–12]. Alternatively, the transport of spin-polarized hot-electron has been proposed to explain ultrafast demagnetization [13–15]. In metals, the pump IR pulses create a strongly out-of-equilibrium electronic distribution called the "nonthermal hot-electron." These nonthermal hot electrons can propagate at the Fermi velocity over tens of nanometers. Due to electron-electron collisions, the nonthermal hot-electron reach an internal equilibrium characterized by a Fermi-Dirac distribution, called "thermal hot-electron." Malinowski *et al.* [13] proposed a ballistic transport of spin-polarized hot electrons as an efficient channel for angular momentum dissipation during the ultrafast demagnetization. Within this model, the different amplitudes and time scales which were experimentally observed have been explained. Recently, Battiato *et al.* proposed a theoretical model in which the demagnetization is entirely explained by the superdiffusive transport of spin-polarized hot-electron [14,15]. This model has been further sustained by experimental results [16–18]. Since then, a plethora of experimental and theoretical works have evidenced that local (such as spin-flip) and nonlocal mechanisms (transport of hot-electron) are both important ingredients to explain the ultrafast magnetization dynamics. Today the controversy lies in the relative importance of the proposed mechanisms [19–22].

Meanwhile, first attempts towards femtosecond spin-transfer torques by ballistic hot electrons have been made by Schellekens *et al.* [23], whereas Choi *et al.* showed that ultrafast spin manipulations can be obtained through electronic thermal transport [24,25]. Such ultrashort hot-electron pulse induced spin manipulations open new routes towards femtosecond spintronics [26]. These potential applications motivate the community to investigate the details of the interactions between the hot-electron pulses and the magnetic layers. Recent studies have now unambiguously confirmed the existence of hot-electron induced ultrafast demagnetization in 3d transition metals [17,27,28,9]. These experiments have reported ultrafast magnetization dynamics induced either by nonthermal hot electrons [9,17] or thermal hot-electron [28]. Unfortunately, it is not straightforward to compare the demagnetization efficiencies induced by nonthermal and thermal hot electrons from those published data since different metals were studied. Furthermore, only the cases of ultrafast demagnetization in 3d elements have been studied.

Previous experiments revealed fundamental dissimilarities in the laser induced ultrafast magnetization dynamics of transition metals (TM) [29] and rare-earth (RE) layers [30]. These differences are related to the localization and hybridization of electron orbitals carrying the spin momentum (respectively the 4f and 3d electrons) and the magnetic anisotropy [30,31]. It is well known that the magnetic transition metals (Ni, Fe, Co) show faster demagnetization than rare-earth elements (Gd, Tb, Dy . . .), a tendency which is also evidenced in RE-TM alloys where this difference is even more intriguing [32–34]. Therefore, the itinerant 3d and localized 4f induced dynamics has been intensively studied in such alloys [34–36]. However,

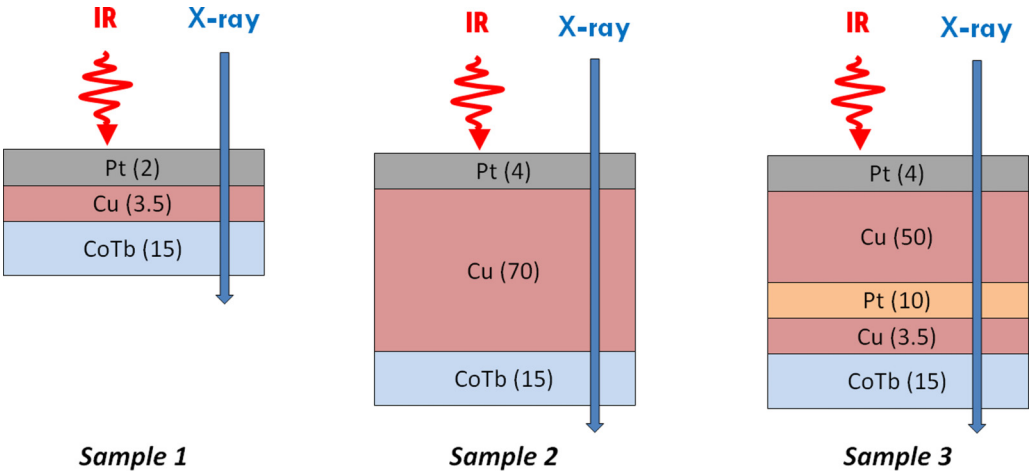

FIG. 1. (a) Sample 1 configuration used as the reference sample and pumped with the IR laser. (b) Sample configurations for sample 2 used to excite the CoTb film with ballistic hot-electron. (c) Sample configurations for sample 3 used to excite the CoTb film with diffusive electrons.

in these alloys the hot-electron induced dynamics is still unexplored. The similarities and differences between IR laser and hot-electron induced $3d$ and $4f$ spin dynamics should give insights into the driving mechanisms in both cases.

In this work, we provide a study of the hot-electron induced dynamics of the $4f$ magnetic moments in a $Co_{74}Tb_{26}$ alloy. For this, we used the element sensitivity of time-resolved x-ray magnetic circular dichroism (XMCD) [33,34]. Furthermore, by comparing the ultrafast demagnetization measured for different samples, we distinguish the specificities of the demagnetization which is induced by nonthermal or by thermal hot-electron. Among other RE-TM alloys, the $Co_{74}Tb_{26}$ alloy is well suited for our study because it shows a fast IR laser induced $4f$ demagnetization dynamics with a short characteristic time of $\tau = 0.28$ ps [33,34]. This fast demagnetization dynamic enhances our sensitivity to other (or additional) excitation sources for which slower dynamics are induced.

II. STATIC AND TIME-RESOLVED EXPERIMENTS

The 15-nm-thick $Co_{74}Tb_{26}$ (label CoTb in the text for commodity) alloys were deposited by dc-magnetron sputtering on Si_3N_4 membranes of 200 nm thickness and capped with three different metallic layers: Pt(2)/Cu(3.5) (sample 1, Fig. 1), Pt(4)/Cu(70) (sample 2, Fig. 1), and Pt(4)/Cu(50)/Pt(10)/Cu(3.5) (sample 3, Fig. 1) (units are in nanometers). In samples 2 and 3, the IR femtosecond laser pulses are absorbed in the Pt(4)/Cu(X) capping layers, generating nonthermal hot-electron pulses, as described by Bergeard *et al.* [9]. According to our calculations, based on the variation of the Poynting vector, the CoTb layers absorb 16.7%, 0.11%, and 0.36% of the incident IR intensity for samples 1, 2, and 3, respectively (method in the Supplemental Material of [9]). Thus, the choice of the different capping layers ensures negligible direct IR excitations in the CoTb alloys for samples 2 and 3 [9]. The thickness of the capping layers is nevertheless limited by the x-ray transmission at the Tb M_5 absorption edge, which is 15% in our experiment. In Cu, the thermalization time of hot electrons is above 500 fs [37]. Therefore, in sample 2, the photoexcited, nonthermal hot electrons can propagate at the Cu Fermi velocity of 0.7 nm/fs towards the $Co_{74}Tb_{26}$ before any thermalization of the hot electrons [38,39]. In sample 3, the additional Pt(10) layer acts as a filter for the nonthermal ballistic hot electrons which are photoexcited in the upper Pt(4)/Cu(50) capping layers. The Pt(10) layer is ideally suited for this purpose because of the low electron attenuation length of ~5 nm [40]. Moreover, the photoexcited hot-electron pulses generated in the upper Pt(4 nm)/Cu(50 nm) drive the electron distribution of the Pt(10) layer in a strongly out-of-equilibrium distribution as efficiently as IR femtosecond laser pulses [41]. The hot electrons are rapidly thermalized, since the electron thermalization time in Pt is much shorter (<200 fs) than those expected in noble metals (>500 fs) [42]. The energy absorbed in the Pt(10) layer is then transferred to the adjacent layers through the heat current mediated by diffusive thermal hot electrons [24]. As a consequence, direct laser excitations are investigated in sample 1, whereas the excitations induced by nonthermal and thermal hot electrons are investigated by comparing the dynamics in samples 2 and 3. To guarantee similar magnetic properties (i.e., anisotropy, magnetic moments) for all samples, we grew a 3.5-nm Cu film on top of the CoTb alloys in samples 1 and 3. Static XMCD spectroscopy has been performed using the ALICE reflectometer at the PM3 beamline at the BESSY II synchrotron radiation source operated by the Helmholtz-Zentrum Berlin [43]. The x-ray absorption spectra (XAS) were measured by monitoring the transmitted x-ray intensities as a function of the photon energy. The x-ray beam and the applied magnetic field of ± 0.7 T were aligned along the sample normal. Two XAS spectra have been recorded with opposite film magnetizations revealing the XMCD at the Tb M_5 edge [Fig. 2(a)]. Hysteresis loops were recorded by tuning the x-ray energy to the Tb M_5 edge [Fig. 2(b)]. These hysteresis evidence square loops and coercive fields of $H_C = 0.33$ T, well below the maximum field of the experimental setup at the FEMTOSPEX end station [44]. Finally, the XMCD measurements show that all samples display almost similar static magnetic properties at the Tb M_5 edge (out-of-plane magnetic anisotropy, square loops, coercive fields, and the values of the magnetic moments) [Figs. 2(a) and 2(b)].

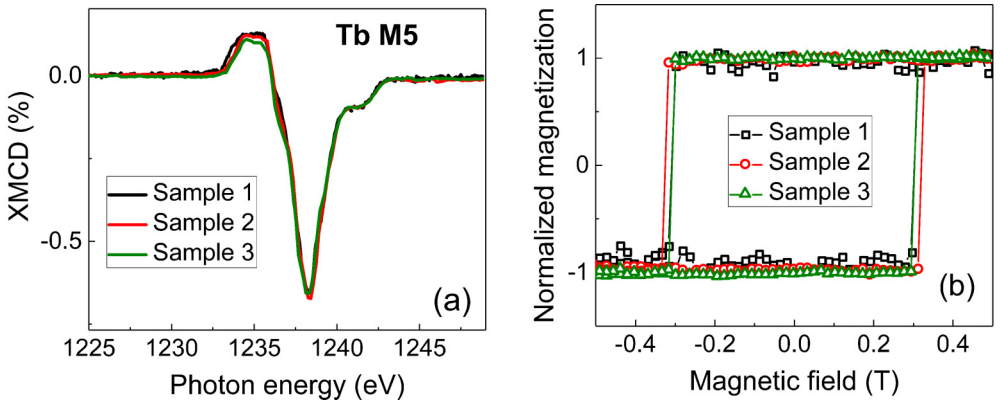

FIG. 2. (a) XMCD spectra at the Tb M_5 edge and (b) hysteresis loops for the samples 1, 2, and 3. The measurements were carried out at $T = 300$ K for a normal incident of the x-ray beam in respect with the sample's surface. XMCD spectra are defined as the difference of XAS spectra obtained for two magnetic field helicities ($H = 0.7$ T). For all samples, the spectra are normalized, such as the amplitude of the isotropic XAS spectrum at the M_5 resonance ($E_{hv} = 1237$ eV) is equal to 1 (the baseline at $E_{hv} = 1220$ eV is equal to 0). Hysteresis loops were acquired by monitoring the x-ray transmission at the Tb M_5 resonance ($E_{hv} = 1237$ eV) as a function of the magnetic field.

The time-resolved XMCD experiments were performed at the femtoslicing beam line of the BESSY II synchrotron radiation source at the Helmholtz-Zentrum Berlin [44]. The experiments were performed in transmission, under an applied magnetic field of ± 0.55 T, using the same geometry as in the static experiments. The experiment requires a pump-probe setup working at 3 kHz, where femtosecond IR laser pulses (3 kHz) were used as the pump while the circularly polarized x-ray pulses (6 kHz) were used as the probe. This procedure allows for probing both the pumped and unpumped transient states. The duration of IR laser and x-ray pulses in the femtoslicing operation mode were 60 fs and 100 fs, respectively, which ensures a global time resolution of $\sim$130 fs [29,31]. The magnetization dynamics have been recorded by monitoring the transmission of the circularly polarized x rays tuned to the core-level absorption edge Tb M_5 as a function of the pump-probe delay. The multisample holder of the experimental chamber allows measuring alternatively from sample 1 (direct pumping by IR pulses) to samples 2 and 3 (indirect excitation). The laser beam diameter of $\sim 500\,\mu$m ensures a homogeneous excitation over the x-ray probed area ($\sim 150\,\mu$m). The laser power was $P = 8$ mW for sample 1 and $P = 24$ mW for sample 2 and sample 3. The cryostat temperature was set to 250 K in order to compensate the laser dc heating, which ensures a base temperature of $T \approx 300$ K at negative delays, well below the temperature of magnetic compensation of the CoTb alloy films ($T_{comp} \approx 550$ K [33]).

III. TIME-RESOLVED EXPERIMENTS

The transient XMCD data recorded at the Tb M_5 edge are shown in Fig. 3 for samples 1, 2, and 3. The ultrafast quenching of the Tb $4f$ magnetic order is observed for all samples. The data are normalized by the XMCD at negative delay and adjusted by classical exponential fits convoluted by a Gaussian function which accounts for the experimental time resolution [31,33,34]. We have characterized the dynamics in the three samples by the following parameters: the demagnetization amplitudes q, the onset of the ultrafast demagnetization t, and the characteristic demagnetization time τ. These parameters, and their error bars, are extracted from the fits and summarized in Table I.

For sample 1, the Tb demagnetization is driven by the direct IR laser excitation and the ultrafast dynamics is used during our experiment as a reference for $t0$. Since the pump conditions have been adjusted to reach almost the same demagnetization amplitude ($q \approx 0.70$) as in our previous work, we will use the characteristic demagnetization time $\tau = 0.28 \pm 0.03$ ps as the reference value for direct IR laser induced demagnetization. We note that the quenching of the magnetic order is reached within the first picosecond after the laser excitation (empty circles in Fig. 3) [33].

For samples 2 and 3, the observed ultrafast Tb demagnetization is not driven by the IR laser excitation. The demagnetization amplitudes and the onset of demagnetization are almost similar for both samples, but the characteristic demagnetization time τ is much larger for sample 3 $\tau = 1.2 \pm 0.4$ ps than for sample 2 $\tau = 0.35 \pm 0.1$ ps (Table I). This difference raises intriguing questions about the origin of the elongation observed when the 10-nm-thick Pt layer is inserted in the thick Cu layer, on top of CoTb. The IR laser power used for the indirect excitations (24 mW) is much larger than the one used for the direct excitation (8 mW). However, the amplitudes of the demagnetization in the CoTb films are only of $q \approx 52\%$ and $q \approx 36\%$ for samples 2 and 3, respectively.

TABLE I. Parameters extracted from the fit functions for the three samples for Tb.

Sample	Demagnetization amplitude q (%)	t (ps)	Characteristic demagnetization time τ (ps)
Sample 1	70 ± 5[a]	0 ± 0.2	0.28 ± 0.03[a]
Sample 2	52 ± 8	0.25 ± 0.2	0.35 ± 0.10
Sample 3	36 ± 6	0.3 ± 0.2	1.2 ± 0.4

[a]The demagnetization amplitude and the characteristic demagnetization time are extracted from López-Flores *et al.* [33].

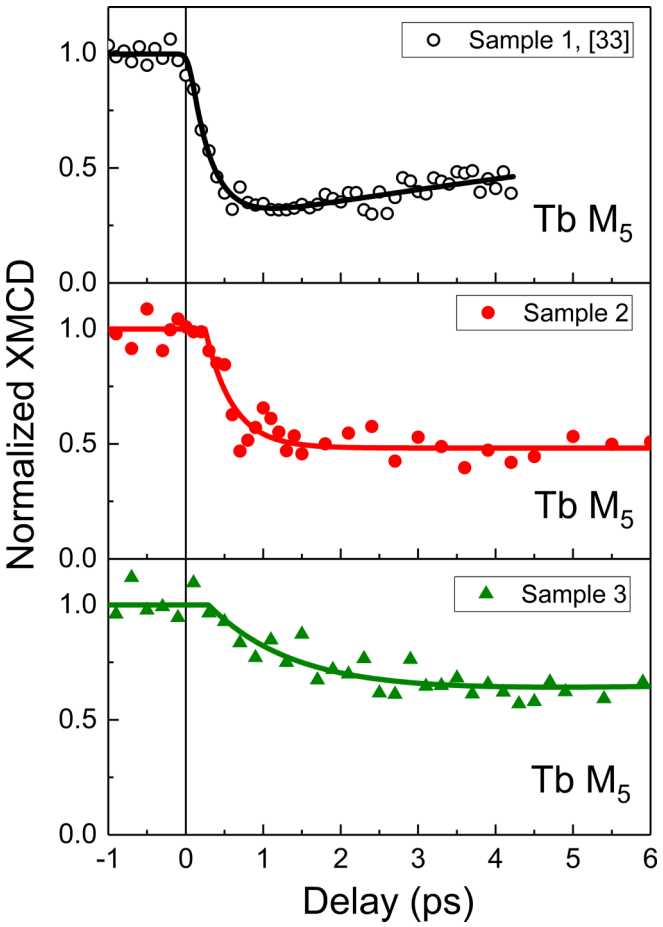

FIG. 3. Transient normalized XMCD at the Tb M_5 edge for samples 1, 2, and 3. For samples 2 and 3, the solid lines are fits in the framework of the three-temperature model. For sample 1, which is used to set the temporal overlap in this experiment, we superpose the data (open circles) and the fit of our previous Tb M_5 dynamics taken in the same experimental configuration [33]. The different sample configurations (samples 1, 2, and 3) show the respective characteristic demagnetization times of $\tau = 0.28 \pm 0.03$ ps, 0.35 ± 0.1 ps, and 1.2 ± 0.4 ps. The data in Fig. 3 (top panel) are reproduced with the authorization of the American Physical Society.

IV. DISCUSSION

It has been shown in the literature that for 3*d* metals the direct laser excitation is not the only excitation process which is able to induce subpicosecond magnetization dynamics [17,27,9,28]. In this work, we extend these conclusions to the case of localized 4*f* magnetic moments in RE-TM alloys. We have used the same capping layers on our RE-TM films as Bergeard *et al.* on their CoPt multilayers [9]. In their work, the onset of the demagnetization is shown to be delayed in the buried magnetic multilayer, with respect to the IR excitation, by ∼120 fs, whereas the characteristic demagnetization time τ is longer by ∼30 fs for a 70-nm Cu capping thickness. The observed elongation of the characteristic demagnetization time τ originates mainly from the spatial elongation of the ballistic transport of nonthermal hot-electron pulses during the propagation towards the ferromagnetic multilayer [9]. Following the description of demagnetization induced by ballistic transport of hot electrons provided by Bergeard *et al.*, the demagnetization onset of the Tb sublattice in sample 2 should be ∼120 fs. This onset of 120 fs is consistent with our experimental value of 250 fs, considering our large error bars (±200 fs).

The demagnetization amplitude in sample 2 is $q = 52\%$ at the Tb M_5 edge, which is large considering the large $Co_{74}Tb_{26}$ film thickness (15 nm) and the limited inelastic mean-free path (IMFP) of the incoming ballistic hot-electron ($\lambda_{up} = 6.5$ nm for majority spins and $\lambda_{down} = 1.2$ nm for the minority spins in Co [40]). We have adapted Eq. (1) from [45] to estimate the in-depth profile of the CoTb excitation by the ballistic hot electrons. We have injected the spin-dependent IMFP instead of IR penetration depth in the formula. We estimate that ∼80% of the incoming ballistic hot electrons with minority spin character are scattered and excite the first 4 nm of the $Co_{74}Tb_{26}$ layer. We also estimate that less than 10% of the incoming ballistic hot electrons with majority spin character reach the bottom of the alloys. The contribution to the demagnetization is described by inelastic scattering of the incoming ballistic non thermal hot electrons with the electrons at the Fermi level of the $Co_{74}Tb_{26}$ alloy. In order to reach $q = 52\%$ with the above-described profile of the ballistic hot electrons, we estimate that the first 3 nm of the CoTb layer should be fully demagnetized, while the demagnetization amplitude in the remaining CoTb layers follows an exponential decay given by the IMFP. Such a scenario could be supported by the 3-times-larger IR fluence used for sample 2 compared to sample 1 (for which 70% demagnetization is observed). However, our estimation neglects the loss of energy at the multiple interfaces of sample 2. Indeed, a large loss of about 40% has been evidenced by Choi *et al.*, who considered the effect for one interface between a noble metal (Au, Cu...) and a metal with a large electron-phonon coupling (Pt, Co...) [41]. It suggests that for sample 2, the scattering of the incoming ballistic hot electrons cannot induce a demagnetization of $q = 52\%$.

Instead we propose that the energy injected by the ballistic nonthermal hot-electron is transported away from the "surface" towards the "bulk" of the $Co_{74}Tb_{26}$ alloy by diffusive nonthermal hot-electron at the Fermi velocity of ∼0.25 nm/fs, as shown by Tas and Maris [45]. The demagnetization is thus described by the multiple scattering events experienced by the nonthermal hot-electron in the $Co_{74}Tb_{26}$ film. Finally, in 3*d* transition metals, both ballistic and diffusive nonthermal hot-electron have been shown to induce ultrafast demagnetizations [9,17]. We propose here that the observed ultrafast demagnetization amplitude at Tb M_5 arises from both the scattering of the incoming ballistic and diffusive nonthermal hot electrons. However, no quantitative estimation can be given, since the multiple electron-scattering processes and the multiple interfaces of the films imply complex theoretical calculations. Therefore we cannot confirm that the incoming ballistic and diffusive nonthermal hot electrons account for the measured demagnetization of $q = 52\%$.

Considering the excitation mechanisms, we know from the literature that the hot electrons excite the 3*d* and 5*d* electrons in the $Co_{74}Tb_{26}$ alloy, similar to IR laser induced ultrafast dynamics in RE layers [30,46] and RE-TM alloys [32–34]. The scattering events experienced by the hot electrons drive the magnetization dynamics, either by producing spin-polarized

superdiffusive hot electrons as claimed by Eschenlohr *et al.* [17] or by inducing spin-flip as claimed by Bergeard *et al* [9]. The demagnetization of the localized $4f$ moments is mediated via the Ruderman-Kittel-Kasuya-Yosida (RKKY) indirect exchange coupling [30,47]. However, the description of the microscopic mechanisms which explain the observed demagnetization is beyond the scope of this article.

Concerning the value of the characteristic demagnetization time $\tau = 350 \pm 100$ fs extracted from sample 2, we note that it is close to the value measured for direct IR excitations in $Co_{74}Tb_{26}$ (sample 1, $\tau = 280 \pm 30$ fs). According to Bergeard *et al.*, the elongation of the ballistic nonthermal hot-electron pulses in our capping layer, compared to the IR pulse, does not exceed 30 fs [9]. The velocity of nonthermal hot electrons (ballistic and diffusive) in Co is ~0.25 nm/fs [48,49]. Therefore, the propagation time of the nonthermal hot electrons in the 15-nm $Co_{74}Tb_{26}$ layer is ~60 fs (15/0.25 = 60 fs), which is well below the characteristic electronic thermalization time of ~100 fs in Co [20]. The nonthermal hot-electron propagation time of 60 fs demonstrates that the different atomic layers in our $Co_{74}Tb_{26}$ film are not simultaneously excited. The difference with the instantaneous excitation induced by IR lasers is due to a notably lower electronic group velocity (~0.25 nm/fs) compared to the speed of light. Adding up the individual contributions, we found a global elongation of the characteristic demagnetization time $\Delta\tau = 90$ fs (stretching in the capping layer 30 fs + propagation time in the $Co_{74}Tb_{26}$ alloy 60 fs). Thus, considering $\tau \approx 280$ fs for direct IR excitation and $\Delta\tau = 90$ fs, we calculate a global demagnetization time of $\tau \approx 370$ fs. We conclude that our value $\tau = 350 \pm 100$ fs measured in sample 2 can be justified by the transport of nonthermal hot electrons towards and within the $Co_{74}Tb_{26}$ film. Finally, we conclude that in sample 2, at the Tb M_5 edge, the ultrafast demagnetization, which is characterized by the demagnetization onset, amplitude, and characteristic time, is consistent with an ultrafast dynamic induced by nonthermal hot electrons.

In order to confirm the possibility to induce ultrafast demagnetization in the Tb $4f$ sublattice by using thermal hot electrons as proposed by Choi *et al.* [41], we performed the pump-probe experiment with sample 3. To compare the efficiency of demagnetization induced by nonthermal or thermal hot electrons we have performed the measurements using the same $Co_{74}Tb_{26}$ alloy but with a specifically designed capping (sample 3). In sample 3, a Pt layer of 10-nm thickness has been inserted between the Pt(4 nm)/Cu(50 nm) and the CoTb alloy layers (Fig. 1) in order to produce a heat current of thermal hot electrons [24]. A demagnetization $q \approx 36\%$ is observed for the same laser power we used for sample 2. Following previous works published by Choi *et al.* [24], we can attribute the demagnetization of sample 3 to the energy transfer from the excited Pt(10) layer towards the CoTb alloy, mediated by diffusive thermal hot electrons. However, a quantitative estimation of the energies injected into the CoTb alloy for samples 2 and 3 is difficult. The energy transported by the hot electrons is dependent on the material and on the interfaces present along the trajectory of the electrons [41]. The presence of additional interfaces in sample 3 (Cu/Pt, Pt/Cu, and Cu/CoTb) may, however, qualitatively explain the reduction of the demagnetization amplitude compared to sample 2 (Cu/CoTb) (sample 3: $q \approx 36\%$ and sample 2: $q \approx 52\%$).

According to Hohlfeld *et al.*, the order of magnitude for the velocity of the diffusive thermal hot electrons in metal is ~0.01 nm/fs [49]. Thus, the propagation time of these electrons in the CoTb 15 nm is ~1.5 ps, in qualitative agreements with our experimental measurements. Therefore, the longer characteristic demagnetization time in sample 3 ($\tau = 1.2 \pm 0.4$ ps) compared to sample 2 ($\tau = 0.35 \pm 0.1$ ps) is qualitatively explained by the slower propagation of thermal diffusive hot electrons. We notice the similarity of our results with the work of Vodungbo *et al.*, who have studied the laser induced demagnetization in Al(40)/CoPd [27], evidencing a 3 times longer characteristic time τ compared to IR excitations. Comparing these results with the work of Salvatella *et al.* suggests that the ultrafast demagnetization of the $3d$ Co in the CoPd film was initiated by thermal hot-electron [28].

The demagnetization onset measured in sample 3 is at 300 ± 200 fs, which is similar, within the error bars, to the onset measured in sample 2. By considering that the demagnetization in sample 3 is caused by the transport of thermal hot electrons from the Pt(10) layer towards the CoTb layer, we can estimate an onset at ~320 fs, which is consistent with our measured value of 300 ± 200 fs. In this calculation, we have considered the following contributions: (i) transport of the photoexcited hot electron in Cu(50) towards the Pt(10) layer (~ + 85 fs) [9]; (ii) thermalization time of the hot electron in Pt(10) (~ + 200 fs [42]); and (iii) heat transport through the Cu(3.5) layer (+35 fs). We use $v = 0.1$ nm/fs for the velocity of the diffusive hot electrons in Cu(3.5), as experimentally measured by Choi *et al* [24]. Different velocities in Cu (0.1 nm/fs) and Co (0.01 nm/fs) [49] are justified by the larger effective mass of the electrons in Co (~7.5 [50]) compared to Cu (~1 [51]).

We point out that the electron attenuation length in Pt is 5 nm [40]. Therefore, we cannot assert that the thermalization of the hot electrons is completed within our 10-nm Pt layer. Thus, we cannot exclude a contribution of residual nonthermal hot electrons to the demagnetization of CoTb in sample 3. However, since in sample 3 we do not observe a fast characteristic demagnetization time close to the value evidenced in sample 2 ($\tau \approx 350$ fs), we can confirm that the contribution of nonthermal hot electrons is very limited. The demagnetization onset induced by such residual nonthermal hot electrons can be estimated to ~113 fs (50 nm Cu + 3.5 nm Cu at 0.7 nm/fs + 10 nm Pt at 0.27 nm/fs) [24,52]. According to our large error bars of ±200 fs for the experimental onset of sample 3 (300 fs), the contribution of nonthermal hot electrons to the onset cannot be identified.

In summary, considering the results from sample 3, we clearly evidence an efficient demagnetization by thermal hot electrons as expected from Choi *et al.* [41]. The signature obtained through the demagnetization characteristic times τ allows discriminating from the nonthermal hot-electron contribution. Finally, considering our results from samples 2 and 3, we show that the quenching of $4f$ magnetic order in CoTb layers can be induced with comparable efficiencies, by nonthermal or thermal hot-electron. The difference in the demagnetization time for sample 2 (~0.35 ps) and sample 3 (~1.2 ps) is qualitatively attributed to the velocity of the

nonthermal and the thermal hot-electron in the CoTb layers (∼1 nm/fs for nonthermal hot electrons and ∼0.01 nm/fs for diffusive thermal hot electrons) [49]. It is worth noting that the speed of sound in Pt is about 2.7 nm/ps. Therefore, we ruled out acoustic phonons triggered by hot-electron [53] as a mechanism for the indirect ultrafast demagnetization in sample 3.

V. CONCLUSIONS

We have reported on a hot-electron induced ultrafast sizable demagnetization of 4*f* magnetic order in CoTb alloys. We provide a qualitative interpretation of our experimental findings based on the transport regime of the hot-electron: either ballistic or diffusive. We show that the demagnetization in the CoTb layer is induced though the transport of nonthermal hot electrons when Pt/ Cu layers are grown on the CoTb film. We further show that a thin 10-nm Pt layer is able to change the ultrafast demagnetization dynamic. The observed dynamic is compatible with thermal hot-electron mediated diffusive heat transport. Qualitative arguments allow us to reproduce the characteristic demagnetization times of $\tau \sim 0.35 \pm 0.10$ ps and $\tau \sim 1.2 \pm 0.4$ ps for both samples.

ACKNOWLEDGMENTS

We are indebted for the scientific and technical support given by N. Pontius, Ch. Schüßler-Langeheine, D. Schick, and R. Mitzner at the slicing facility at the BESSY II storage ring. The ALICE project was supported by BMBF Contract No. 05K10PC2. The authors are grateful for financial support received from the following agencies: the French "Agence National de la Recherche" via Project No. ANR-11-LABX-0058_NIE and Project EQUIPEX UNION No. ANR-10-EQPX-52, the CNRS-PICS program, the EU Contract Integrated Infrastructure Initiative I3 in FP6 Project No. R II 3CT-2004-50600008. Experiments were carried out on the IJL Project TUBE-Davms equipment funded by FEDER (EU), PIA (Programme Investissemnet d'Avenir), Region Grand Est, Metropole Grand Nancy, and ICEEL.

[1] J. Stohr and H. C. Siegmann, *From Fundamentals to Nanoscale Dynamics* (Springer-Verlag, Berlin, 2006).
[2] E. Beaurepaire, J.-C. Merle, A. Daunois, and J.-Y. Bigot, Phys. Rev. Lett. **76**, 4250 (1996).
[3] A. Kirilyuk, A. V. Kimel, and T. Rasing, Rev. Mod. Phys. **82**, 2731 (2010).
[4] B. Koopmans, G. Malinowski, F. Dalla Longa, D. Steiauf, M. Fähnle, T. Roth, M. Cinchetti, and M. Aeschlimann, Nat. Mater. **9**, 259 (2010).
[5] K. C. Kuiper, G. Malinowski, F. Dalla Longa, and B. Koopmans, J. Appl. Phys. **109**, 07D316 (2011).
[6] T. Roth, A. J. Schellekens, S. Alebrand, O. Schmitt, D. Steil, B. Koopmans, M. Cinchetti, and M. Aeschlimann, Phys. Rev. X **2**, 021006 (2012).
[7] S. Günther, C. Spezzani, R. Ciprian, C. Grazioli, B. Ressel, M. Coreno, L. Poletto, P. Miotti, M. Sacchi, G. Panaccione *et al.*, Phys. Rev. B **90**, 180407 (2014).
[8] A. J. Schellekens and B. Koopmans, Phys. Rev. B **87**, 020407 (2013).
[9] N. Bergeard, M. Hehn, S. Mangin, G. Lengaigne, F. Montaigne, M. L. M. Lalieu, B. Koopmans, and G. Malinowski, Phys. Rev. Lett. **117**, 147203 (2016).
[10] K. Carva, M. Battiato, and P. M. Oppeneer, Phys. Rev. Lett. **107**, 207201 (2011).
[11] K. Carva, M. Battiato, D. Legut, and P. M. Oppeneer, Phys. Rev. B **87**, 184425 (2013).
[12] S. Essert and H. C. Schneider, J. Appl. Phys. **111**, 07C514 (2012).
[13] G. Malinowski, F. Della Longa, J. H. H. Rietjens, P. V. Paluskar, R. Huijink, H. J. M. Swagten, and B. Koopmans, Nat. Phys. **4**, 855 (2008).
[14] M. Battiato, K. Carva, and P. M. Oppeneer, Phys. Rev. Lett. **105**, 027203 (2010).
[15] M. Battiato, K. Carva, and P. M. Oppeneer, Phys. Rev. B **86**, 024404 (2012).
[16] A. Melnikov, I. Razdolski, T. O. Wehling, E. T. Papaioannou, V. Roddatis, P. Fumagalli, O. Aktsipetrov, A. I. Lichtenstein, and U. Bovensiepen, Phys. Rev. Lett. **107**, 076601 (2011).
[17] A. Eschenlohr, M. Battiato, P. Maldonado, N. Pontius, T. Kachel, K. Holldack, R. Mitzner, A. Föhlisch, P. M. Oppeneer, and C. Stamm, Nat. Mater. **12**, 332 (2013).
[18] C. E. Graves, A. H. Reid, T. Wang, B. Wu, S. de Jong, K. Vahaplar, I. Radu, D. P. Bernstein, M. Messerschmidt, L. Müller *et al.*, Nat. Mater. **12**, 293 (2013).
[19] E. Turgut, C. La-o-vorakiat, J. M. Shaw, P. Grychtol, H. T. Nembach, D. Rudolf, R. Adam, M. Aeschlimann, C. M. Schneider, T. J. Silva *et al.*, Phys. Rev. Lett. **110**, 197201 (2013).
[20] J. Wieczorek, A. Eschenlohr, B. Weidtmann, M. Rösner, N. Bergeard, A. Tarasevitch, T. O. Wehling, and U. Bovensiepen, Phys. Rev. B **92**, 174410 (2015).
[21] E. Jal, V. López-Flores, N. Pontius, T. Ferté, N. Bergeard, C. Boeglin, B. Vodungbo, J. Lüning, and N. Jaouen, Phys. Rev. B **95**, 184422 (2017).
[22] J.-Y. Chen, L. He, J.-P. Wang, and M. Li, Appl. Phys. Lett. **110**, 092407 (2017).
[23] A. J. Schellekens, K. C. Kuiper, R. R. J. C. de Wit, and B. Koopmans, Nat. Commun. **5**, 4333 (2014).
[24] G.-M. Choi, B.-C. Min, K.-J. Lee, and D. G. Cahill, Nat. Commun. **5**, 4334 (2014).
[25] G.-M. Choi, C.-H. Moon, B.-C. Min, K.-J. Lee, and D. G. Cahill, Nat. Phys. **11**, 576 (2015).
[26] J. Walowski and M. Münzenberg, J. Appl. Phys. **120**, 140901 (2016).
[27] B. Vodungbo, B. Tudu, J. Perron, R. Delaunay, L. Müller, M. H. Berntsen, G. Grübel, G. Malinowski, C. Weier, J. Gautier *et al.*, Sci. Rep. **6**, 18970 (2016).
[28] G. Salvatella, R. Gort, K. Bühlmann, S. Däster, A. Vaterlaus, and Y. Acremann, Struct. Dyn. **3**, 055101 (2016).
[29] C. Stamm, T. Kachel, N. Pontius, R. Mitzner, T. Quast, K. Holldack, S. Khan, C. Lupulescu, E. F. Aziz, M. Wiestruck *et al.*, Nat. Mater. **6**, 740 (2007).
[30] M. Wietstruk, A. Melnikov, C. Stamm, T. Kachel, N. Pontius, M. Sultan, C. Gahl, M. Weinelt, H. A. Dürr, and U. Bovensiepen, Phys. Rev. Lett. **106**, 127401 (2011).

[31] C. Boeglin, E. Beaurepaire, V. Halté, V. López-Flores, C. Stamm, N. Pontius, H. A. Dürr, and J.-Y. Bigot, Nature (London) **465**, 458 (2010).
[32] I. Radu, K. Vahaplar, C. Stamm, T. Kachel, N. Pontius, H. A. Dürr, T. A. Ostler, J. Barker, R. F. L. Evans, R. W. Chantrell *et al.*, Nature (London) **472**, 205 (2011).
[33] V. López-Flores, N. Bergeard, V. Halté, C. Stamm, N. Pontius, M. Hehn, E. Otero, E. Beaurepaire, and C. Boeglin, Phys. Rev. B **87**, 214412 (2013).
[34] N. Bergeard, V. López-Flores, V. Halté, M. Hehn, C. Stamm, N. Pontius, E. Beaurepaire, and C. Boeglin, Nat. Commun. **5**, 3466 (2014).
[35] I. Radu, C. Stamm, A. Eschenlohr, F. Radu, R. Abrudan, K. Vahaplar, T. Kachel, N. Pontius, R. Mitzner, K. Holldack *et al.*, SPIN **5**, 1550004 (2015).
[36] T. Ferté, N. Bergeard, L. Le Guyader, M. Hehn, G. Malinowski, E. Terrier, E. Otero, K. Holldack, N. Pontuis, and C. Boeglin, Phys. Rev. B **96**, 134303 (2017).
[37] X. Shen, Y. P. Timalsina, T.-M. Lu, and M. Yamaguchi, Phys. Rev. B **91**, 045129 (2015).
[38] S. D. Brorson, J. G. Fujimoto, and E. P. Ippen, Phys. Rev. Lett. **59**, 1962 (1987).
[39] T. Juhasz, H. E. Elsayed-Ali, G. O. Smith, C. Suárez, and W. E. Bron, Phys. Rev. B **48**, 15488 (1993).
[40] V. P. Zhukov, E. V. Chulkov, and P. M. Echenique, Phys. Rev. B **73**, 125105 (2006).
[41] G.-M. Choi, R. B. Wilson, and D. G. Cahill, Phys. Rev. B **89**, 064307 (2014).
[42] C. Lei, M. Bauer, K. Read, R. Tobey, Y. Liu, T. Popmintchev, M. M. Murname, and H. C. Kapteyn, Phys. Rev. B **66**, 245420 (2002).
[43] R. Abrudan, F. Brüssing, R. Salikhov, J. Meermann, I. Radu, H. Ryll, F. Radu, and H. Zabel, Rev. Sci. Instrum. **86**, 063902 (2015).
[44] K. Holldack, J. Bahrdt, A. Balzer, U. Bovensiepen, M. Brzhezinskaya, A. Erko, A. Eschenlohr, R. Follath, A. Frisov, W. Frentrup *et al.*, J. Synchrotron Radiat. **21**, 1090 (2014).
[45] G. Tas and H. J. Maris, Phys. Rev. B **49**, 15046 (1994).
[46] A. Eschenlohr, M. Sultan, A. Melnikov, N. Bergeard, J. Wieczorek, T. Kachel, C. Stamm, and U. Bovensiepen, Phys. Rev. B **89**, 214423 (2014).
[47] I. A. Campbell, J. Phys. F **2**, L47 (1972).
[48] D. Gall, J. Appl. Phys. **119**, 085101 (2016).
[49] J. Hohlfeld, S.-S. Wellershoff, J. Güdde, U. Conrad, V. Jähnke, and E. Matthias, Chem. Phys. **251**, 237 (2000).
[50] S. Wakoh, D. M. Edwards, and E. P. Wohlfarth, J. Phys. Colloques **32**, C1-1073 (1971).
[51] S. O. Kasap, *Principles of Electronic Materials and Devices*, 2nd ed. (McGraw-Hill, New York, 2002).
[52] D. H. Dye, J. B. Ketterson, and G. W. Crabtree, J. Low Temp. Phys. **30**, 813 (1978).
[53] M. Lejman, V. Shalagatskyi, O. Kovalenko, T. Pezeril, V. V. Temnov, and P. Ruello, J. Opt. Soc. Am. B **31**, 282 (2014).